Validity boundary of orbital-free molecular dynamics method corresponding to thermal ionization of shell structure

Chang Gao,[1,2] Shen Zhang,[1,3] Wei Kang,[1,3,4,*] Cong Wang,[1,5] Ping Zhang,[1,4,5,†] and X. T. He[1,4,5,‡]

[1]*Center for Applied Physics and Technology, HEDPS, Peking University, Beijing 100871, China*

[2]*School of Physics, Peking University, Beijing 100871, China*

[3]*College of Engineering, Peking University, Beijing 100871, China*

[4]*IFSA Collaborative Innovation Center of MoE, Peking University, Beijing 100871, China*

[5]*Institute of Applied Physics and Computational Mathematics, Beijing 100088, China*

(Received 7 September 2016; published 9 November 2016)

With ^{6}Li D as an example, we show that the applicable region of the orbital-free molecular dynamics (OFMD) method in a large temperature range is determined by the thermal ionization process of bound electrons in shell structures. The validity boundary of the OFMD method is defined roughly by the balance point of the average thermal energy of an electron and the ionization energy of the lowest localized electronic state. This theoretical proposition is based on the observation that the deviation of the OFMD method originates from its less accurate description to the charge density in partially ionized shells, as compared with the results of the extended first-principles molecular dynamics method, which well reproduces the charge density of shell structures.

DOI: 10.1103/PhysRevB.94.205115

I. INTRODUCTION

The development of first-principles methods, including the first-principles molecular dynamics (FPMD) method [1–5], the orbital-free molecular dynamics (OFMD) method [6,7], and the path-integral Monte Carlo (PIMC) method [8,9], affords a possible theoretical approach without experimental inputs to determine important material properties of dense plasmas to a considerable accuracy. These material properties, e.g., the equation of state (EOS) [10,11], transport coefficients [7,12,13], and opacities [14], play a fundamental role in the development of high energy density physics [15], stellar physics [16], planet physics [17], and inertial confinement fusion (ICF) [18].

There are very few cases that one can rely on only one of these methods to calculate the property of a certain material in a large range of density and temperature, e.g., from nearly 0 K to hundreds of electron volts [15] or from usual solid density to over 1000 times the solid density [18,19], which are typical conditions frequently met in warm dense matter (WDM) experiments [20,21] and ICF implosions [18,22]. This kind of calculation can be done, however, by the combination of two or several of the first-principles methods, each of which covers a relatively small region in the phase space. This combined method has become a common practice recently and has been successfully applied to the calculation of EOS and transport properties for a variety of materials [7,23–26].

An important issue of the combined approach is the validity boundary of each method in the combination. It determines how the results of different methods connect to each other. In this work we focus on the validity boundary of the OFMD method in the OFMD+FPMD combination, which has been extensively used to calculate material properties of low Z plasmas [26,27] and recently has been extended to the calculation of multicomponent plasmas [28,29] and high Z materials [30]. There are several proposals [27–29,31–33] available on how to bridge the OFMD method and the FPMD method. To make a further development of the combined method, a clear physical picture to the validity boundary is necessary.

With the extended first-principles molecular dynamics (ext-FPMD) method developed recently [34], which greatly expands the application region of the traditional FPMD method, we show how the OFMD results deviate from the FPMD results, using ^{6}Li D as an illustrating example. Our results display that around the maximum compression ratio of ^{6}Li D along its principal Hugoniot, thermal properties of ^{6}Li D are mainly determined by the thermal ionization process of the $1s$ electronic state of the lithium (Li) element, where the pressure ionization effects associated with the change of density [15] are less important. It thus provides a suitable situation to illustrate the validity boundary corresponding to the thermal ionization of localized electronic states. It shows that the OFMD method is applicable when the average thermal energy k_BT is greater than the ionization energy I_{Lowest} of the lowest bound electronic state, where k_B is the Boltzmann constant, and T is the temperature of electrons. This condition can be explicitly expressed as $k_BT/I_{\text{Lowest}} > 1$.

The rest of this paper is composed of three sections. In Sec. II, we briefly summarize the OFMD method and the ext-FPMD method. Also described are computational details of the calculation. In Sec. III, a comparison of the codes is done on the resulting principal Hugoniots, EOS, and charge densities, from which the validity criterion of the OFMD method is extracted. In Sec. IV, we give a short discussion to conclude this paper. All formulas hereafter are presented in the atomic units with the Boltzmann constant k_B set to be 1. In numerical results, electron volt (eV) or Rydberg (Ry) is used as the unit of temperature and energy following the convention.

II. METHODOLOGY AND COMPUTATIONAL DETAILS

Both methods, i.e., the OFMD and ext-FPMD methods, divide the motion of ions and electrons adiabatically via

*weikang@pku.edu.cn

†zhang_ping@iapcm.ac.cn

‡xthe@iapcm.ac.cn

the Born-Oppenheimer approximation [35]. Trajectories of ions are determined by solving Newton's equation of motion with the force between ions calculated through the Hellman-Feynman's force theorem or its finite-temperature generalization [36,37]. The motion of electrons in both methods is treated quantum mechanically, however, in slightly different styles.

In the OFMD method, the density of electrons n is determined where the total free energy F_e reaches its minimum. F_e can be written as a functional form of n as $F_e[n] = T_K[n,\beta] + U_{ee}[n] + U_{ei}[n] + F_{xc}[n]$, where β is the inverse of temperature, $T_K[n,\beta]$ is the finite-temperature kinetic contribution of electrons to the free energy, U_{ee} is the Hartree energy between electrons, U_{ei} is the electron-ion interaction, and F_{xc} is the exchange-correlation interaction. The kinetic contribution $T_K[n,\beta]$, which is composed of an entropic contribution and the kinetic energy, is calculated through the Thomas-Fermi approximation as

$$T_K[n,\beta] = \frac{1}{\beta}\int d\mathbf{r}\left\{n(\mathbf{r})\phi(\mathbf{r}) - \frac{2\sqrt{2}}{3\pi^2\beta^{3/2}} I_{3/2}[\phi(\mathbf{r})]\right\}, \quad (1)$$

where I_ν is the Fermi integral of order ν, and $\phi(\mathbf{r})$ is related to the intrinsic chemical potential μ_0 through $\phi(\mathbf{r}) = \beta\mu_0$. The von Weizsäcker gradient correction [38] is neglected because of its minor contribution to the EOS [26,27,39], as long as thermal ionization of localized electronic states is concerned.

The FPMD method is based on Mermin's finite-temperature density functional theory (FT-DFT) [40]. The electronic wave functions $\psi_i(\mathbf{r})$ are described by Kohn-Sham equations [41,42] $\hat{H}_{\rm KS}\psi_i = \epsilon_i\psi_i$ with

$$\hat{H}_{\rm KS} = -\tfrac{1}{2}\nabla^2 + V_H[n] + V_{xc}[n] + V_{ei}[n],$$

where the subscript i denotes the ith electron, ϵ_i is the corresponding eigenenergy, V_H is the Hartree potential from other electrons, V_{xc} is the exchange-correlation potential, and V_{ei} is the electron-ion interaction.

The ext-FPMD method [34] extends the FPMD method to a much higher temperature limit by replacing the wave functions of high energy electrons with plane waves. It further leads to an analytical form of density of state (DOS) $D(\epsilon) = \frac{\sqrt{2}\Omega}{\pi^2}\sqrt{\epsilon - U_0}$ for high energy electrons, with which the high-energy-electron correction to charge density, total energy, and entropy can be explicitly written as integrals

$$n_{\rm corr}(\mathbf{r}) = \frac{1}{\Omega}\int_{E_c}^{\infty} d\epsilon f(\epsilon)D(\epsilon),$$

$$E_{\rm corr} = \int_{E_c}^{\infty} d\epsilon f(\epsilon)D(\epsilon)(\epsilon - U_0),$$

and

$$S_{\rm corr} = -\int_{E_c}^{\infty} d\epsilon D(\epsilon)\{f(\epsilon)\ln f(\epsilon) + [1 - f(\epsilon)]\ln[1 - f(\epsilon)]\}.$$

Here, ϵ is the energy, Ω is the volume, U_0 is the constant background potential, E_c is the starting energy of the plane-wave approximation, and $f(\epsilon)$ is the Fermi-Dirac distribution.

All simulations are carried out in a periodic cubic box containing 128 atoms, i.e., 64 formula units of ^{6}Li D. The OFMD calculations are performed using the ABINIT package [43,44], while the ext-FPMD calculations are carried out with an implementation of the method [34] based on the QUANTUM ESPRESSO package [45].

For a given temperature and density, the time step to move the ions is determined by a scaling form [13] of $\delta t \sim 1/(\rho^{1/3}T^{1/2})$, and δt ranges from 0.01 fs to 0.1 fs in the simulations. Trajectories of the last 4000 steps are used to calculate the required physical properties statistically after the system has evolved for 6000 steps, which makes the numerical error of total energy and pressure less than 1%. In both methods, the Perdew-Zunger parametrization [46] of the local density approximation (LDA) to the exchange-correlation interaction is employed. Preceding studies have shown [34] that the influence of different exchange-correlation functionals is small and thus not considered in the paper.

The electron-ion interaction in the OFMD simulations is represented by the norm-conserving regularization form of the original Troullier-Martins (TM) prescription [47] with a core cutoff radius 0.5 Bohr for both lithium and deuterium elements. It differs slightly from the norm-conserving regularization proposed in Ref. [24]. In the TM process, the electronic charge density used in the unscreening is generated in a full quantum mechanical calculation, while the one used in Ref. [24] is calculated from the Thomas-Fermi model. Nevertheless, the difference in EOS resulting from these two regularizations is minor, as will be further illustrated in the following section. The plane wave cutoff energy to represent charge density is set to be 300 Ry.

In the ext-FPMD simulations, the electron-ion interactions in the projected-augmented-wave (PAW) [48] format are generated using the ATOMPAW program [49], which also have a core cutoff radius of 0.5 Bohr. The plane wave cutoff energy is set to be 200 Ry. A shifted $2 \times 2 \times 2$ Monkhorst-Pack [50] mesh is used to sample the Brillouin zone. 800 bands are explicitly included in calculations, where the 160 bands at the top are used to determine the value of U_0, as required by the ext-FPMD method [34]. In addition, atomic calculations are also performed with the ATOMPAW program, from which the average radius of a given electronic orbital is determined.

III. RESULTS AND DISCUSSION

The validity boundary problem is well illustrated in the principal Hugoniot of ^{6}Li D [28,34], where the "bump" structure is attributed to the shell structure of electrons [34,51] and its shape sensitively depends on the accuracy of pressure and total energy in the calculation. There were other OFMD investigations which also paid attention to the shell structure of electrons and its influence on the validity boundary of the OFMD method [27,52], however, not examined in the same manner.

Figure 1(a) displays principal Hugoniots of ^{6}Li D calculated with the OFMD method and the ext-FPMD method, focused on the region around the maximum compression ratio $\eta \sim 4.3$. The states along the principal Hugoniot satisfy the Rankin-Hugoniot relation $E_1 - E_0 = \frac{1}{2}(P_1 + P_0)(V_0 - V_1)$, where E is the total internal energy per formula unit, P is the pressure, and V is the volume of each ^{6}Li D formula unit. Subscripts 0 and 1 stand for the uncompressed and the shocked states, respectively. The initial state of ^{6}Li D is a face-centered cubic (FCC) lattice structure at $\rho_0 = 0.8$ g/cm^3, and the initial

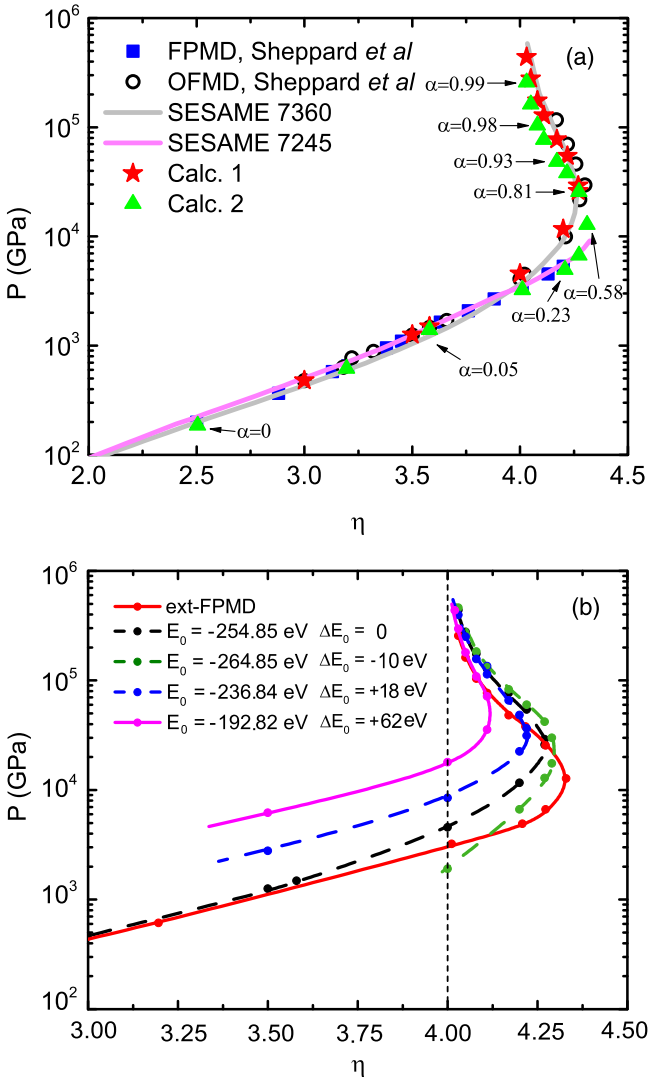

FIG. 1. (a) Principal Hugoniots of ^{6}Li D calculated by using the OFMD method (Calc. 1) and the ext-FPMD method (Calc. 2), compared with preceding OFMD results [28] and SESAME 7360 [28], SESAME 7245 [28]. Ionization ratio α of the 1s state of the lithium element along the ext-FPMD Hugoniot is also displayed. (b) OFMD Hugoniots calculated with different E_0, where the red solid curve is the ext-FPMD result, and the black curve is Calc. 1 in (a).

pressure $P_0 \approx 0$. The equation is solved with the second order polynomial interpolation.

The OFMD Hugoniot, displayed as stars and denoted as Calc. 1 in the figure, is calculated with $E_0 = -254.85$ eV per formula unit. It agrees with the OFMD result of Ref. [28], displayed as hollow circles. The small difference between Calc. 1 and the previous OFMD results comes from technical details, as have been described in Sec. II. The ext-FPMD Hugoniot, displayed as upper triangles and denoted as Calc. 2, is calculated with the initial energy E_0 of -217.70 eV per formula unit. It serves as the reference and keeps the same as the LDA result in Ref. [34].

As displayed in Fig. 1(a), Calc. 1 (the OFMD result) separates from Calc. 2 (the ext-FPMD result) when pressure is greater than 4 TPa. The maximum compression ratio of Calc. 1 is smaller than that of Calc. 2. At the same compression ratio η, the pressure of Calc. 1 in the lower branch of the "bump" is 40–150% higher than that in Calc. 2 near the maximum η. For instance, at $\eta = 4.20$ the pressure of Calc. 1 is 11.67 TPa, while the pressure of Calc. 2 is 4.95 TPa, which is half of the magnitude of Calc. 1.

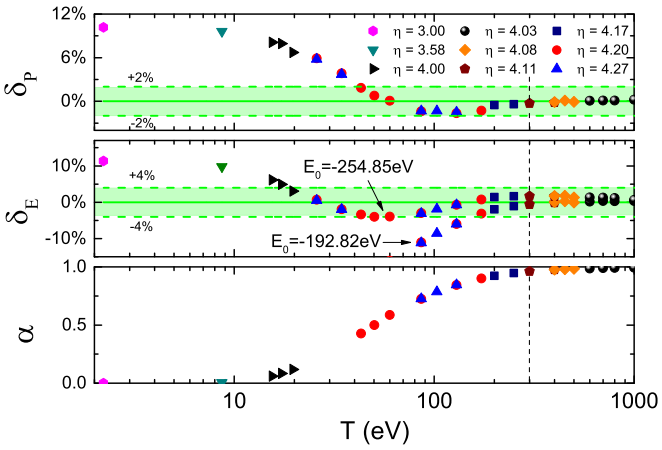

FIG. 2. Relative deviation of pressure (δ_P) and energy difference (δ_E) of OFMD calculations with respect to the ext-FPMD results. In the subfigure of δ_E, results calculated with $E_0 = -254.85$ eV and $E_0 = -192.82$ eV are displayed. As a reference, ionization ratios of the corresponding thermal states are displayed together.

The choice of E_0 is a major issue in the combined calculation of the OFMD+FPMD method [26,28]. In order to show that the variation of E_0 is not the origin of the difference between the OFMD Hugoniot and the reference calculation of the ext-FPMD method, several modified E_0 are used to rebuild the Hugoniot in the OFMD calculation. Figure 1(b) displays the change of Hugoniots with the variation of E_0. The black line denotes the OFMD Hugoniot calculated with $E_0 = -254.85$ eV per formula unit, and the red line denotes the reference calculation from the ext-FPMD method. When E_0 increases, the maximum η decreases and the size of the "bump" structure shrinks, which makes the Hugoniot further deviate from the ext-FPMD calculation. On the other hand, when E_0 decreases, the pressure at low compression ratio is much smaller than the ext-FPMD pressure. Anyhow, there is no way to recover the entire ext-FPMD results by modifying E_0.

The other factor that determines the Hugoniot is the EOS. In order to make the Hugoniots close to each other, the pressure difference between the two methods in the shocked state at a given density (or η equivalently) needs to be small enough, and the total energy can only have a constant difference from each other, as required by the Rankine-Hugoniot relation. So, in this sense, the difference in the principal Hugoniot sensitively reflects the variation of EOS in the two methods.

Using the ext-FPMD results as a reference, the relative difference of pressure can be defined as $\delta_P = (P_{\text{OFMD}} - P_{\text{ext-FPMD}})/P_{\text{ext-FPMD}}$. Figure 2(a) displays the relative difference in the pressure calculation, presented as a function of temperature. Data calculated at different η (in the range from 3.0 to 4.27) are distinguished with various symbols, as indicated in the legend. The relative difference δ_P is not sensitive to the change of η but has a prompt response to

the variation of temperature in the compression ratio range considered. The variation of δ_P can be divided into two regions. In the first region, δ_P keeps decreasing from ∼10% at low temperature to ∼−2% at $T \sim 100$ eV. In the second region, where $T > 100$ eV, δ_P slightly increases and approaches zero.

Similarly, the relative deviation of $\Delta E = E - E_0$ in the Rankin-Hugoniot relation can be defined as $\delta_E = (\Delta E_{\text{OFMD}} - \Delta E_{\text{ext-FPMD}})/\Delta E_{\text{ext-FPMD}}$. In the compression ratio range considered, it is essentially a function of temperature and less relevant to the change of η, as displayed in Fig. 2(b). δ_E strongly depends on the choice of E_0 in the calculation. When calculated with $E_0 = -254.85$ eV per formula unit, δ_E displays a damped undulating structure. However, when δ_E is calculated with $E_0 = -192.82$ eV per formula unit, which corresponds to the curve of $\Delta E_0 = +62$ eV per formula unit in Fig. 1(b), δ_E is less than −100% at low temperature and monotonically approaches zero. Note that the low temperature part of the curve is out of the range of δ_E displayed. Although δ_E displays a different trend at low temperature, it approaches zero at high temperature in both cases. This is a reasonable result because $|E_0| \ll |E|$ at high temperature limit, at which E_0 can be neglected in the Rankin-Hugoniot relation.

Taking both P and $E - E_0$ into consideration, it is clear that the EOS from the OFMD calculation below at least 180 eV is out of the validity boundary of the method, provided one takes the green area as a loose standard, at which $|\delta_P| = 2\%$ and $|\delta_E| = 4\%$. When Hugoniot calculation is concerned, it is safe to use the Hugoniot state $\eta = 4.11$ and $T = 300$ eV, indicated by the vertical line in Fig. 2, as the starting point of the OFMD calculation, where both $|\delta_P|$ and $|\delta_E|$ is less than 1%. The corresponding E_0 is −192.82 eV per formula unit. With this value, the OFMD Hugoniot agrees with the upper branch of the ext-FPMD Hugoniot, as displayed by the purple curve in Fig. 1(b).

Following the procedure described above, the validity boundary of the OFMD method can be practically determined. However, one can go a step further to understand the physical origin of the deviations.

Figure 3 displays the density of states (DOS) of electrons and the projected DOS (PDOS) of the 1s orbital of Li for selected states around $\eta = 4$, calculated with the ext-FPMD method. It shows that the 1s electronic orbital of Li, represented by the PDOS in the figure, is energetically separated from other electronic orbitals at relatively low temperature. With the increase of temperature, the distribution of the 1s state smears out, and the peak of the PDOS moves to a lower energy due to the increase of the valence state β in ionic $Li^{\beta+}$. Atomic calculations show that the 1s has an average radius less than 0.5 Bohr, which is 1/6 of the average distance (∼3 Bohr) between atoms at $\eta \sim 4$. This suggests that the ionization potential depression (IPD), which mainly depends on the density [53], is not strong enough to delocalize the majority of the 1s state, and the "bump" structure in the Hugoniot is more likely caused by the thermal ionization of the 1s state of the lithium element. Note that some of the 1s states of Li are indeed energetically overlapped with other electronic states at high temperature, as displayed in Fig. 3(d). It occurs when an extremely high local density emerges somewhere in the system as a result of strong thermal fluctuations, where the distance between ions is comparable with the average radius of the 1s orbital of Li.

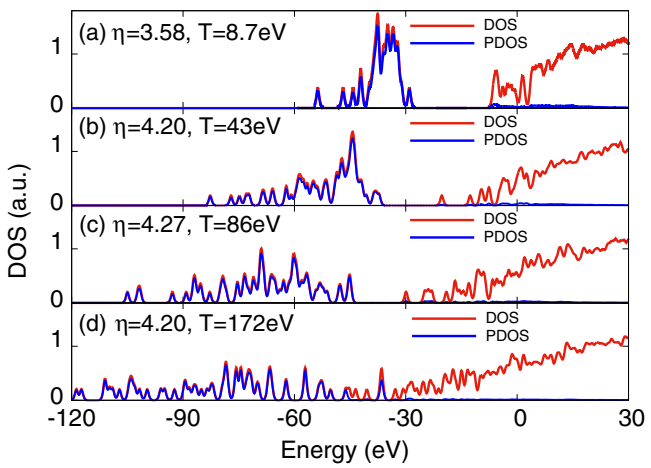

FIG. 3. Density of electronic states and projected density of states of the 1s state of Li for selected ^{6}Li D thermal states along the Hugoniot curves.

Thermal ionization can be quantitatively represented by the average ionization ratio α of the 1s state of Li, which is calculated using the ext-FPMD method in the work to be the average energy of the lowest band in Fig. 3. As displayed in the bottom panel of Fig. 2, it monotonically increases from 0 to 1 with the temperature. In order to establish the relation between the "bump" structure and the thermal ionization, the average ionization ratio α is explicitly displayed along the principal Hugoniot in Fig. 1(a). It shows that the formation of the "bump" structure closely follows the ionization process of the 1s electronic state of Li. At $\eta = 3.58$, α is 0.05, which indicates that the thermal state is near the starting point of the ionization process. Then, the 1s state is about half ionized ($\alpha = 0.58$) when the Hugoniot reaches its maximum compression ratio $\eta = 4.31$. When the ionization process finishes, the compression ratio η approaches the $\eta = 4$ limit of strong shock waves. This well supports the conjecture that the thermal ionization of the 1s state of Li is the main cause of the "bump" structure.

The deviation of P and $E - E_0$ also depends on α. This is evident when the three quantities are put together, as displayed in Fig. 2. It is noticeable that the deviation in P and $E - E_0$ vanishes when most of the electrons in the bound 1s state of Li are ionized.

The origin of the deviation between the two methods can be further illustrated by comparing the charge density. In the framework of FT-DFT, which is the foundation of both methods, all thermal properties, including total energy, pressure, and stresses, at a given temperature are determined by the charge density distribution. Difference in charge density may be well presented as deviations in thermal properties. In order to illustrate the variation originated from methodologies, charge densities are calculated on the same atomic configurations extracted from equilibrium trajectories of a given equilibrium state.

Figure 4 displays typical charge density distribution along the line connecting two ions. Note that only charge densities outside of the pseudopotential cutoff radius ($r_c = 0.5$ Bohr in our calculations) are displayed. In Figs. 4 (a)–4(c), charge densities on the lines connecting two lithium ions, two

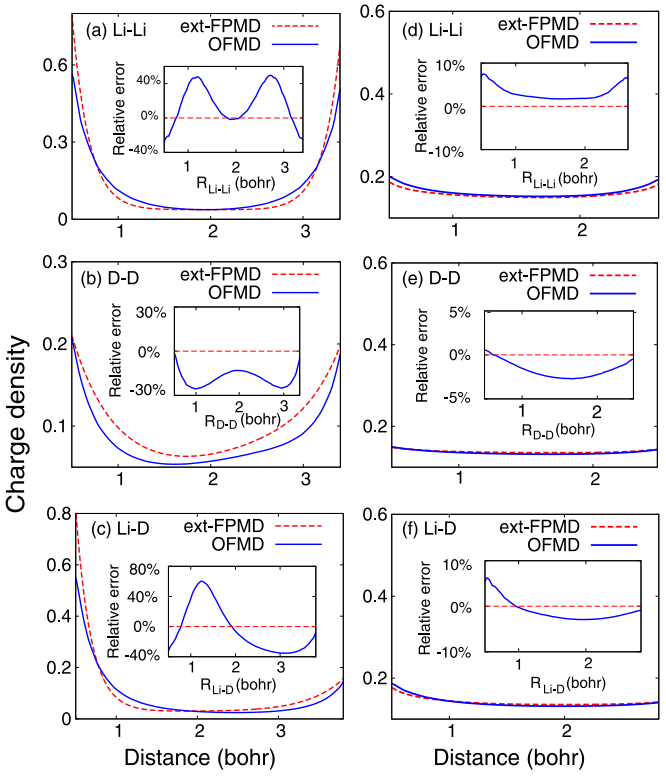

FIG. 4. Typical charge density distribution along the line connecting two ions, calculated from the OFMD method and the ext-FPMD method. (a)–(c) Charge density distribution in the thermal state $\eta = 3.00$ and $T = 2.22$ eV. (d)–(f) Charge density distribution in the thermal state $\eta = 4.11$ and $T = 300$ eV.

deuterium ions, as well as one lithium ion and one deuterium atom, are presented respectively, which are calculated at a given ionic configuration in the Hugoniot state of $\eta = 3.00$ and $T = 2.22$ eV. The corresponding α for the $1s$ state of Li is almost zero, i.e., most of the electrons in the $1s$ state are not ionized. Charge densities calculated with the two methods are distinguished by different colors and line styles, as indicated in the legend.

In this case, the charge density has a significant difference between the two methods. Compared with the ext-FPMD charge density distribution, the OFMD method underestimates the charge around the ions. The charge density near the Li ions is underestimated by about 20–30%, and in the interstitial space, the OFMD charge density fluctuates around the ext-FPMD charge density. The amplitude of the fluctuation can be as much as 60%, for example, in Fig. 4(c). This deviation in charge density gives a reasonable account to the deviation in thermal properties displayed in Fig. 2.

On the other hand, when most of the $1s$ electrons of Li are ionized, charge densities calculated with the two methods are close to each other. Figures 4(d)–4(f) give an illustration to this situation. They are calculated in the Hugoniot state of $\eta = 4.11$ and $T = 300$ eV, corresponding to the connecting point of the combined OFMD+FPMD method. The difference of charge density in all three cases is less than 8%, which is much smaller than those in Figs. 4(a)–4(c). The corresponding difference of pressure is -0.27%, and the deviation of $E - E_0$ is about -0.57%.

The comparison of charge density shows that the accuracy of the OFMD method essentially depends on how well the charge density distribution is reproduced. At low temperature, electrons of bound states are distributed in shell structures, which are not well reproduced by the OFMD method [54]. However, when temperature is greater than the ionization energy of the lowest bound states, which is the $1s$ state of Li here, the majority of electrons are ionized and the influence of the shell structure is negligible. At this time the OFMD method can describe the electronic charge density distribution well and can thus calculate thermal properties accurately.

As thermal ionization of the shell structure is concerned, an approximate validity boundary of the OFMD method may be suggested as $T \sim I_{\mathrm{Lowest}}$. It varies with the density as the result of the IPD effect. Considering the fluctuation of density in the system, I_{Lowest} smears out on the scale of energy, as displayed in Fig. 3. The I_{Lowest} presented is then an average of the system.

In the calculation of Hugoniots, this condition gives an estimation to the temperature range at the connecting point. For example, $I_{\mathrm{Lowest}} = 94$ eV in ^{6}Li D, and the connecting temperature is $T = 300$ eV. For aluminum, of which electrons are distributed in several shells, the I_{Lowest} is determined to be about 2100 eV, and the connecting point has a temperature of $T = 2400$ eV. A notable situation is the material at extremely high density, where all bound states of electrons disappear due to IPD. In this case, the OFMD method has the largest validity range.

IV. CONCLUDING REMARKS

With the ^{6}Li D as an example, we have shown that the OFMD method has a large deviation in the description of electronic structures and thermal properties in the system made of bound and unbound electrons, compared with the ext-FPMD calculation. Most of the deviations come from the shell structure of bound electrons, which may essentially define a validity boundary $T \sim I_{\mathrm{Lowest}}$ for the OFMD method in the calculation of dense plasmas. We note that this validity boundary is relevant when thermal properties in a large temperature range are concerned. It is not contradicted with current efforts of searching for orbital-free density functionals of improved performance [55,56], which usually focus on zero temperature or in a small temperature range. Because the electronic charge density of bound states has a small variation in the range, the influence of these electrons can be described by a well designed pseudopotential [57–60] or by an optimized functional to the kinetic energy [33,61].

ACKNOWLEDGMENTS

This work is financially supported by the Science Challenge Project (Grant No. JCKY2016212A501), the NSFC (Grant Nos. 11274019 and 11275032) and NSAF (Grant Nos. U1530113 and U1530258). Part of the calculations were supported by the Special Program for Applied Research on Super Computation of the NSFC-Guangdong Joint Fund (the second phase).

[1] G. Galli, R. Q. Hood, A. U. Hazi, and F. Gygi, Phys. Rev. B **61**, 909 (2000).

[2] T. J. Lenosky, S. R. Bickham, J. D. Kress, and L. A. Collins, Phys. Rev. B **61**, 1 (2000).

[3] M. P. Surh, T. W. Barbee, and L. H. Yang, Phys. Rev. Lett. **86**, 5958 (2001).

[4] S. Zhao, S. Zhang, W. Kang, Z. Li, P. Zhang, and X.-T. He, Phys. Plasmas **22**, 062707 (2015).

[5] S. Zhang, S. Zhao, W. Kang, P. Zhang, and X.-T. He, Phys. Rev. B **93**, 115114 (2016).

[6] F. Lambert, J. Clérouin, and S. Mazevet, EPL **75**, 681 (2006).

[7] C. Wang, X.-T. He, and P. Zhang, Phys. Rev. Lett. **106**, 145002 (2011).

[8] D. M. Ceperley, Rev. Mod. Phys. **67**, 279 (1995).

[9] B. Militzer and D. M. Ceperley, Phys. Rev. Lett. **85**, 1890 (2000).

[10] S. X. Hu, B. Militzer, V. N. Goncharov, and S. Skupsky, Phys. Rev. Lett. **104**, 235003 (2010).

[11] S. X. Hu, B. Militzer, V. N. Goncharov, and S. Skupsky, Phys. Rev. B **84**, 224109 (2011).

[12] B. Holst, R. Redmer, and M. P. Desjarlais, Phys. Rev. B **77**, 184201 (2008).

[13] L. Burakovsky, C. Ticknor, J. D. Kress, L. A. Collins, and F. Lambert, Phys. Rev. E **87**, 023104 (2013).

[14] C. Wang, X.-T. He, and P. Zhang, Phys. Plasmas **19**, 042702 (2012).

[15] R. P. Drake, *High-Energy-Density Physics: Fundamentals, Inertial Fusion, and Experimental Astrophysics* (Springer, Berlin, 2006).

[16] T. Guillot, Science **286**, 72 (1999).

[17] A. Laio, S. Bernard, G. L. Chiarotti, S. Scandolo, and E. Tosatti, Science **287**, 1027 (2000).

[18] J. Lindl, Phys. Plasmas **2**, 3933 (1995).

[19] S. Atzeni and J. Meyer-ter Vehn, *The Physics of Inertial Fusion* (Claerendon Press, Oxford, 2004).

[20] S. M. Vinko, O. Ciricosta, B. I. Cho, K. Engelhorn, H. K. Chung, C. R. D. Brown, T. Burian, J. Chalupsky, R. W. Falcone, C. Graves, V. Hajkova, A. Higginbotham, L. Juha, J. Krzywinski, H. J. Lee, M. Messerschmidt, C. D. Murphy, Y. Ping, A. Scherz, W. Schlotter, S. Toleikis, J. J. Turner, L. Vysin, T. Wang, B. Wu, U. Zastrau, D. Zhu, R. W. Lee, P. A. Heimann, B. Nagler, and J. S. Wark, Nature (London) **482**, 59 (2012).

[21] D. J. Hoarty, P. Allan, S. F. James, C. R. D. Brown, L. M. R. Hobbs, M. P. Hill, J. W. O. Harris, J. Morton, M. G. Brookes, R. Shepherd, J. Dunn, H. Chen, E. Von Marley, P. Beiersdorfer, H. K. Chung, R. W. Lee, G. Brown, and J. Emig, Phys. Rev. Lett. **110**, 265003 (2013).

[22] X. T. He, J. W. Li, Z. F. Fan, L. F. Wang, J. Liu, K. Lan, J. F. Wu, and W. H. Ye, Phys. Plasmas **23**, 082706 (2016).

[23] B. Militzer, Phys. Rev. Lett. **97**, 175501 (2006).

[24] F. Lambert, J. Clérouin, and G. Zérah, Phys. Rev. E **73**, 016403 (2006).

[25] V. Recoules, F. Lambert, A. Decoster, B. Canaud, and J. Clérouin, Phys. Rev. Lett. **102**, 075002 (2009).

[26] C. Wang and P. Zhang, Phys. Plasmas **20**, 092703 (2013).

[27] J.-F. Danel, L. Kazandjian, and G. Zérah, Phys. Plasmas **19**, 122712 (2012).

[28] D. Sheppard, J. D. Kress, S. Crockett, L. A. Collins, and M. P. Desjarlais, Phys. Rev. E **90**, 063314 (2014).

[29] T. Sjostrom and S. Crockett, Phys. Rev. B **92**, 115104 (2015).

[30] J.-F. Danel, P. Blottiau, L. Kazandjian, R. Piron, and M. Torrent, Phys. Plasmas **21**, 102701 (2014).

[31] C. Wang, Y. Long, X.-T. He, J.-F. Wu, W.-H. Ye, and P. Zhang, Phys. Rev. E **88**, 013106 (2013).

[32] S. X. Hu, L. A. Collins, T. R. Boehly, J. D. Kress, V. N. Goncharov, and S. Skupsky, Phys. Rev. E **89**, 043105 (2014).

[33] T. Sjostrom and J. Daligault, Phys. Rev. Lett. **113**, 155006 (2014).

[34] S. Zhang, H. Wang, W. Kang, P. Zhang, and X. T. He, Phys. Plasmas **23**, 042707 (2016).

[35] G. Kresse and J. Hafner, Phys. Rev. B **47**, 558 (1993).

[36] R. M. Martin, *Electronic Structure: Basic Theory and Practical Methods* (Cambridge University Press, Cambridge, 2004).

[37] C. Kittel and H. Kroemer, *Thermal physics* (W. H. Freeman and Company, New York, 1980).

[38] F. Perrot, Phys. Rev. A **20**, 586 (1979).

[39] G. Zérah, J. Clérouin, and E. L. Pollock, Phys. Rev. Lett. **69**, 446 (1992).

[40] N. D. Mermin, Phys. Rev. **137**, A1441 (1965).

[41] P. Hohenberg and W. Kohn, Phys. Rev. **136**, B864 (1964).

[42] W. Kohn and L. J. Sham, Phys. Rev. **140**, A1133 (1965).

[43] X. Gonze, J.-M. Beuken, R. Caracas, F. Detraux, M. Fuchs, G.-M. Rignanese, L. Sindic, M. Verstraete, G. Zerah, F. Jollet, M. Torrent, A. Roy, M. Mikami, P. Ghosez, J.-Y. Raty, and D. Allan, Comput. Mater. Sci. **25**, 478 (2002).

[44] X. Gonze, B. Amadon, P.-M. Anglade, J.-M. Beuken, F. Bottin, P. Boulanger, F. Bruneval, D. Caliste, R. Caracas, M. Côté, T. Deutsch, L. Genovese, P. Ghosez, M. Giantomassi, S. Goedecker, D. Hamann, P. Hermet, F. Jollet, G. Jomard, S. Leroux, M. Mancini, S. Mazevet, M. Oliveira, G. Onida, Y. Pouillon, T. Rangel, G.-M. Rignanese, D. Sangalli, R. Shaltaf, M. Torrent, M. Verstraete, G. Zerah, and J. Zwanziger, Comp. Phys. Commun. **180**, 2582 (2009).

[45] P. Giannozzi, S. Baroni, N. Bonini, M. Calandra, R. Car, C. Cavazzoni, D. Ceresoli, G. L. Chiarotti, M. Cococcioni, I. Dabo, A. D. Corso, S. de Gironcoli, S. Fabris, G. Fratesi, R. Gebauer, U. Gerstmann, C. Gougoussis, A. Kokalj, M. Lazzeri, L. Martin-Samos, N. Marzari, F. Mauri, R. Mazzarello, S. Paolini, A. Pasquarello, L. Paulatto, C. Sbraccia, S. Scandolo, G. Sclauzero, A. P. Seitsonen, A. Smogunov, P. Umari, and R. M. Wentzcovitch, J. Phys.: Condens. Matter **21**, 395502 (2009).

[46] J. P. Perdew and A. Zunger, Phys. Rev. B **23**, 5048 (1981).

[47] N. Troullier and J. L. Martins, Phys. Rev. B **43**, 1993 (1991).

[48] P. E. Blöchl, Phys. Rev. B **50**, 17953 (1994).

[49] N. Holzwarth, A. Tackett, and G. Matthews, Comp. Phys. Commun. **135**, 329 (2001).

[50] H. J. Monkhorst and J. D. Pack, Phys. Rev. B **13**, 5188 (1976).

[51] B. F. Rozsnyai, J. R. Albritton, D. A. Young, V. N. Sonnad, and D. A. Liberman, Phys. Lett. A **291**, 226 (2001).

[52] M. S. Murillo, J. Weisheit, S. B. Hansen, and M. W. C. Dharma-wardana, Phys. Rev. E **87**, 063113 (2013).

[53] W. Kang, S. Zhao, S. Zhang, P. Zhang, Q. F. Chen, and X.-T. He, Sci. Rep. **6**, 20623 (2016).

[54] V. Karasiev and S. Trickey, Comp. Phys. Commun. **183**, 2519 (2012).

[55] V. V. Karasiev, D. Chakraborty, O. A. Shukruto, and S. B. Trickey, Phys. Rev. B **88**, 161108 (2013).

[56] T. G. White, S. Richardson, B. J. B. Crowley, L. K. Pattison, J. W. O. Harris, and G. Gregori, Phys. Rev. Lett. **111**, 175002 (2013).

[57] B. Zhou, Y. Alexander Wang, and E. A. Carter, Phys. Rev. B **69**, 125109 (2004).

[58] Y. Ke, F. Libisch, J. Xia, L.-W. Wang, and E. A. Carter, Phys. Rev. Lett. **111**, 066402 (2013).

[59] J. Lehtomäki, I. Makkonen, M. A. Caro, A. Harju, and O. Lopez-Acevedo, J. Chem. Phys. **141**, 234102 (2014).

[60] W. Mi, S. Zhang, Y. Wang, Y. Ma, and M. Miao, J. Chem. Phys. **144**, 134108 (2016).

[61] Y. A. Wang, N. Govind, and E. A. Carter, Phys. Rev. B **60**, 16350 (1999).